

The role of surface oxygen vacancies in BiVO_4

Wennie Wang,[†] Patrick James Strohbeen,[‡] Dongho Lee,[¶] Chenyu Zhou,^{§,||} Jason Ken Kawasaki,[‡] Kyoung-Shin Choi,[¶] Mingzhao Liu,[§] and Giulia Galli^{*,†,⊥,#}

[†]*Pritzker School of Molecular Engineering, University of Chicago, Chicago, IL 60637, USA*

[‡]*Materials Science and Engineering, University of Wisconsin-Madison, Madison, WI 53706, USA*

[¶]*Department of Chemistry, University of Wisconsin-Madison, Madison, WI 53706, USA*

[§]*Center for Functional Nanomaterials, Brookhaven National Laboratory, Upton, NY 11973, USA*

^{||}*Department of Materials Science and Chemical Engineering, Stony Brook University, Stony Brook, NY 11794*

[⊥]*Materials Science Division and Center for Molecular Engineering, Argonne National Laboratory, Lemont, Illinois 60439, USA*

[#]*Department of Chemistry, University of Chicago, Chicago, IL 60615, USA*

E-mail: gagalli@uchicago.edu

Abstract

Bismuth vanadate (BiVO_4) is a widely-studied oxide in solar water splitting, known for its ease of synthesis, high charge extraction yields, and advantageous band alignment with water. We present a combined first-principles and experimental study of the electronic structure of the (010) surface of BiVO_4 aimed at disentangling the impact of surface and bulk oxygen vacancies on the electronic structure and transport properties. We found that oxygen vacancies are deep donors at the surface as they are in the bulk; our calculations on defect and polaron formation energies suggest that while polarons

formed from oxygen vacancies in the bulk can contribute to conductivity, those at the surface likely do not. Our results also show that out-of-plane structural relaxations at the surface contribute to the relatively immobile nature of electron polarons derived from surface oxygen vacancies. The structural model derived from first-principles calculation was validated by comparing computed results with experimental measurements of single-crystal and epitaxially-grown single-crystalline BiVO₄ samples. We also found reasonably good agreement between our calculated and measured work functions for BiVO₄ samples with and without oxygen vacancies.

1 Introduction

Solar water splitting is a renewable means for generating hydrogen fuel and a widely attractive avenue for clean energy.¹⁻⁸ Hence the search for optimal photoelectrodes is an active field of research. At minimum an ideal photoelectrode should be stable in aqueous conditions, have a band gap in the visible, favorable band edge positions for water reduction and/or oxidation, and efficient electron-hole separation. *n*-type BiVO₄ has emerged as a promising material candidate that satisfies many of the aforementioned criteria for water splitting. BiVO₄ photoanodes are relatively inexpensive and facile to synthesize,⁹ in addition to being fairly stable against photoelectrochemical and chemical corrosion.^{9,10} Furthermore, the conduction band is closely aligned with the H₂ evolution potential.¹¹⁻¹³ Perhaps most advantageous, as a photoanode BiVO₄ has a large (over 70%) electron-hole separation yield at a potential as low as 0.6 V vs reversible hydrogen electrode¹⁴ and a favorable photovoltage of ≈ 1 V for water oxidation.¹⁰ While the reported band gap (2.4-2.6 eV^{11,14-16}) is slightly too large to absorb a large fraction of the solar spectrum with high radiation flux,¹⁷ the band gap can be reduced via e.g., doping with nitrogen¹⁴ or pairing BiVO₄ with *n*-type semiconductors of smaller band gaps.¹⁸

Owing to these advantages, various efforts have been made to improve the photoelectrochemical behavior of BiVO₄.^{14,19-24} One such effort is to better understand the charge

transport properties. Conductivity in BiVO_4 predominantly occurs through small polaron hopping,^{25–28} and the formation of small polarons is closely tied with that of oxygen vacancies, which are ubiquitous in oxides and can dramatically alter the electronic and atomic structure of the host solid. Consequently several studies have proposed various mechanisms in which oxygen vacancies may play a role in transport properties.^{14,20–22}

Yet, the influence of polarons and oxygen vacancies on photoelectrochemical properties remains elusive. Whether the presence of oxygen vacancies hinders or helps the transport properties of BiVO_4 is still a controversial topic. For instance, Qiu et al.²⁹ reported better electron diffusivities and photocurrent densities for samples with lower oxygen vacancy concentration grown via electrodeposition. Qiu et al. attributed the improved conductivity in samples with lower oxygen vacancy concentration to the fact that oxygen vacancies may act as trap and recombination sites. In direct contrast, Zhang et al.³⁰ reported an improved electron conductivity for samples of higher oxygen vacancy concentration grown via pulsed laser deposition under a reducing carbon monoxide environment. These contrasting studies highlight the need to understand the role of oxygen vacancies in samples obtained from disparate growth and preparation methods.

In order to understand the microscopic role of defects on photoelectrochemical properties, we turn to computational studies. Several calculations have been carried out to characterize the pristine bulk in which no defects are present, including calculations of electronic structure and optical properties,^{12,31–34} transport properties,^{26,35} and electronic behavior of polarons in the bulk.^{36,37} For example, using hybrid functional molecular dynamics, Wiktor et al. found that at finite temperature the electron and hole polaron levels in the bulk are more than 1.0 eV from the H^+/H_2 and $\text{H}_2\text{O}/\text{O}_2$ redox potentials, respectively,³⁷ suggesting favorable recombination of electron-hole polaron states. In the case of the defective bulk, computational studies have reported conflicting results on bulk oxygen vacancies, describing them as shallow centers in some density functional theory (DFT) studies^{38,39} and as deep centers in other DFT investigations with standard functionals²⁰ and with hybrid functionals.²¹ Thus

far, these computational studies have mostly focused on the bulk or pristine surface.

However, the electronic structure and the morphology of photo-absorbing surfaces and interfacial chemistry naturally play a critical role in the photoelectrochemical activity. Different surface facets and terminations can have markedly varied chemistry and physics, e.g. they may act differently in separating the photon-generated electron-hole pairs.^{40–42} Based on computed free-energy profiles of oxygen evolution reaction pathways and adsorption energies,^{22,43} the presence of oxygen vacancies at the surface has been proposed to improve water splitting through increasing the number of active adsorption sites and potentially enhancing charge transfer. However, other studies have suggested that oxygen vacancies can primarily act as recombination centers and traps.⁴⁴ Investigations based on nudged elastic band calculations on oxygen migration suggested that vacancies mostly contribute to bulk conductivity.⁴⁵ Several computational studies have also considered the presence of water on BiVO₄ surfaces, either as adsorbed species,^{46,47} as a frozen-liquid,^{41,48} by both utilizing a solvation model⁴⁶ or an explicit solvent;⁴⁹ however, these studies assumed a pristine surface.

Despite an increasing number of insights coming from theory and computation, the role of oxygen vacancies in the bulk and at the surface of BiVO₄ remains controversial, and at best unclear. A systematic atomistic study on oxygen vacancies in relation to small polaron formation, particularly at the surface, appears to be essential to build a holistic understanding of the properties of BiVO₄ and thus achieve an efficient means towards generating clean hydrogen fuel. There are several open questions worth investigating: What is the level of first-principles theory needed to describe the surface of BiVO₄? What is the role of surface relaxation? How do oxygen vacancies at the surface differ from those in the bulk (e.g., in polaron formation energy and charge states)? How do surface polarons differ from those in the bulk? How do we bridge the comparison between our calculations on single-crystalline structures and experimental photoelectrochemical devices based on polycrystalline materials? In this work, we aim to address these questions for the (010) BiVO₄ surface and provide the groundwork for future studies on interfaces with water. We focus on (010), which is one

of the most energetically favorable facets, for both epitaxial single-crystalline samples grown using the methodology from Refs. 27 and 30 and single crystals as previously reported in Ref. 11. We use first-principles methods and validate the structural model derived computationally by comparing calculated and experimentally-determined band edges and work functions. We compare our calculations with previously reported band alignment and work function measurements on single-crystalline samples¹¹ and with the work function we measured using single-crystalline epitaxial samples with a well-defined surface and composition. The epitaxial samples serve as a bridge between single-crystalline samples and polycrystalline samples that are used in devices, and ultimately in future studies will allow for more meaningful comparisons between our calculations and polycrystalline BiVO₄.

The rest of the paper is organized as follows. The computational and experimental methodologies are presented in Sections 2 and 3, respectively. After introducing our results for the bulk in Section 4, we present an analysis on the structural relaxation of the pristine surface in Section 5. This is followed with band edge and work function calculations, with benchmarks using several levels of theory. We demonstrate that semi-local functionals have serendipitous agreement with experiment, and hybrid functionals are needed to accurately describe the band edges at finite temperature. We then introduce oxygen vacancies to the surface, investigating the stability of several surface polaron configurations and defect formation energies in Section 6. Our results indicate that a polaron arising from a surface oxygen vacancy is a deep donor whose electronic levels are well separated from the band edges and from the polaron levels at the pristine surface and in the bulk. Thus, unlike in the bulk, such defect polaron states are expected to contribute little to conductivity, but instead may serve as possible recombination centers. Next we compare work functions between single-crystalline epitaxially-grown samples and calculated slabs of BiVO₄ with and without oxygen vacancies. Finally, we conclude by discussing the broader impact of our results for the study of photo-electrochemical performance.

2 Computational Methodology

Our calculations are based on first-principles density functional theory (DFT) within the Kohn-Sham framework.^{50,51} We use a plane-wave basis sets and norm-conserving pseudo-potentials^{52,53} with a 90 Ry energy cutoff. The valence electrons are $6p^36s^25d^{10}$, $3d^34s^23p^63s^2$ and $2p^42s^2$ for Bi, V and O, respectively. All bulk properties are obtained with a $4 \times 4 \times 2$ k -point mesh; we verified that a larger mesh of $6 \times 6 \times 4$ leads to < 0.5 meV difference in total energies. Forces on bulk structures are converged within 50 meV/Å. Our calculations were carried out with the QUANTUM ESPRESSO code.^{54,55}

As BiVO₄ is non-magnetic, we use DFT+U_{eff}⁵⁶ with U_{eff} = (U-J) = 2.7 eV applied to the vanadium 3d states.⁵⁷ This value of U was previously tested for bulk BiVO₄.^{14,21} We also used the dielectric-dependent hybrid (DDH) functional as described in Ref. 58, which showed DDH yields more robust band gaps across several elemental and binary compounds compared to the general gradient approximation and hybrid functionals with standard mixing $\alpha = 0.25$. In DDH, the Hartree-Fock mixing parameter $\alpha = 1/\epsilon_\infty = 1/6.9 = 0.145$ equals the inverse of the high-frequency dielectric constant,^{14,21} obtained using density functional perturbation theory. A comparison of our calculated bulk parameters with those reported in the literature may be found in the Supplementary Information (SI).

While several choices of surface cleavage are possible, we focus on the lowest energy surface. We generated symmetric slabs⁵⁹ using a 24-atom $I2/b$ cell with tetragonal lattice parameters, which is related to the conventional monoclinic $C2/c$ cell via a change-of-basis transformation.⁹ Each slab consists of at least 20 Å of vacuum and a minimum of 8 atomic layers (see SI for convergence tests). Previous reports²¹ have found the monoclinic and tetragonal lattice parameters yield comparable defect electronic structure and formation energies in the bulk. Similarly we find that using tetragonal lattice parameters is a reasonable approximation to the monoclinic cell for slab calculations; the computed band gaps differ by < 0.05 eV, the work function by < 0.1 eV, and band edges by < 0.05 eV. In the $C2/c$ cell, the lowest energy surface is the (010) plane (equivalent to the (001) surface in the $I2/b$ cell).

We henceforth refer to this surface as the (010) surface.

In order to simulate the presence of an oxygen vacancy at the surface, an oxygen atom is removed within the first two layers from the surface (see Section 5) of a $2 \times 2 \times 2$ slab supercell and calculated with a $2 \times 2 \times 1$ k -point mesh. In the case of Mo-doping considered for comparison with work function measurements, we substitute one V for Mo for each atomic percent concentration. We verified that a $4 \times 4 \times 1$ k -point mesh leads to total energy differences on the order of 1 meV. Spin polarization is included in our calculations and all defect or slab geometry forces are converged to within 100 meV/Å.

2.1 Defect Formation Energies

We calculate the defect formation energy for oxygen vacancies near the surface in order to investigate their thermodynamic stability and compare with their corresponding properties in the bulk. The formation energy of an oxygen vacancy is defined as⁶⁰

$$E^f[V_O] = E_{\text{tot}}[V_O^q] - E_{\text{tot}}[\text{BiVO}_4] - \mu_O + qE_F + \Delta^q, \quad (1)$$

where $E_{\text{tot}}[V_O^q]$ is the total energy of a slab supercell containing the oxygen vacancy, $E_{\text{tot}}[\text{BiVO}_4]$ is the total energy of the pristine slab, and μ_O is the chemical potential of oxygen. The Fermi level E_F is referenced to the valence-band maximum (VBM) of the bulk. The term Δ^q is a charge-state dependent correction due to the finite size of the supercell,⁶⁰ which allows for the extraction of the defect properties in the dilute limit. We follow the method proposed by Freysoldt et al.⁶¹ to compute the Δ^q in two-dimensional systems. Further discussion on the calculated chemical potentials and comparison of our calculated heat of formation enthalpies with literature and experimental results may be found in the SI.

3 Experimental Methodology

Epitaxial BiVO_4 thin films with (010)-orientation (with respect to the $C2/c$ cell) are grown by pulsed laser deposition (PLD) over (001) yttria-stabilized zirconia (cubic, $a = 5.145 \text{ \AA}$) substrates with an epitaxial indium tin oxide (cubic, $a = 10.127 \text{ \AA}$) buffer layer as the bottom electrical contact, at conditions similar to those of Refs. 28 and 27. We prepared undoped as-grown epitaxial samples in which the laser ablation target is made of stoichiometric BiVO_4 . Measurement details on the photo-emission spectroscopy and work function determination are provided in the SI.

4 Bulk Properties

We begin with a brief description of the bulk properties computed at three levels of theory: semi-local density functional theory (DFT), DFT+U, and dielectric-dependent hybrid functionals (DDH⁵⁸). As shown in Figure 1, the crystal structure of BiVO_4 consists of 4-fold tetrahedrally coordinated vanadium atoms, which are corner-sharing with 8-fold dodecahedrally coordinated bismuth atoms. The bulk electronic properties have been studied at great length,^{11,12,32,62} and here we highlight key features. The bulk V-O bond length is 1.74 \AA in DFT+U (1.72 \AA in DDH); the bulk Bi-O lengths range between 2.51 and 2.45 \AA (2.44 and 2.49 \AA in DDH).

Similar to many other transition metal oxides, the occupied electronic states of BiVO_4 have predominantly O $2p$ character whereas the unoccupied states have mostly transition metal character, i.e, V $3d$. Salient features are the non-negligible contribution of the Bi p orbitals to the conduction bands and the s -character at the top of the valence states arising from the lone pair on Bi, which is frequently invoked to have a key role in photo-electrochemical activity.^{16,63,64} The relative position of electronic states stemming from Bi, V, and O as found in our calculations has been corroborated extensively with molecular orbital theory³² and near edge x-ray absorption fine structure measurements (NEXAFS).¹¹

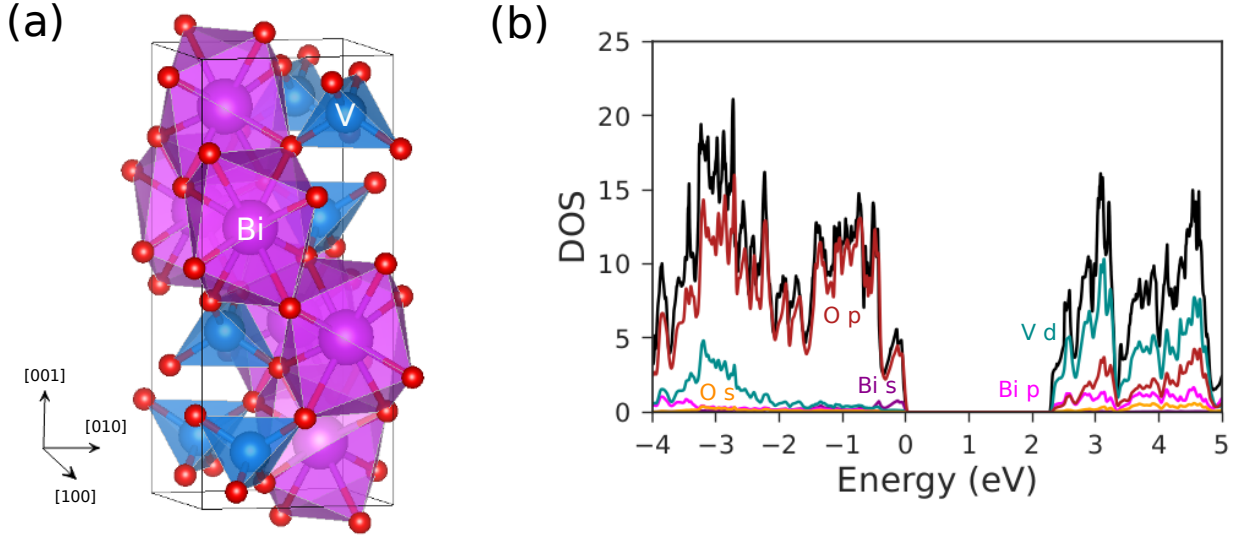


Figure 1: (a) Crystal structure of BiVO₄ with bismuth atoms in purple, vanadium atoms in blue, and oxygen atoms in red. (b) The corresponding total (black) and projected (colored) density of states. The valence band maximum is referenced to zero.

A detailed summary of bulk lattice parameters and band gaps may be found in the SI. Overall, there is fair agreement between calculated lattice parameters at the DFT, DFT+U and DDH levels of theory with at most 0.8% error relative to experiment. Interestingly, the DDH lattice parameters computed at T=0 appear to exhibit the largest error, when compared to experiment. However, as discussed below, this is likely due to significant temperature renormalization effects.

The fundamental band gap (defined as the difference between the conduction and valence band edges) at the DFT+U level is ~ 2.27 eV (3.44 eV in DDH), which is an apparent underestimation (large overestimation in DDH) of the experimental value (~ 2.4 - 2.6 eV^{11,14-16}) (see SI). However, it is known that temperature renormalization (which is not captured in our 0 K DFT calculations) is significant. Using path-integral molecular dynamics simulations (PIMD), Wiktor et al.³⁴ evaluated the total renormalization of the fundamental band gap at room temperature [including spin-orbit coupling (SOC), which comes primarily from Bi and lowers the band gap by 0.13 eV]; they reported values of 0.70 eV for semilocal functionals and 1.05 eV for PBE0. While a finite temperature study is beyond the scope of this paper,

in Section 5.2 we shall use a rigid band shift as an ad-hoc correction to demonstrate the influence of temperature corrections on band alignment.

5 Pristine (010) Surface

5.1 Surface relaxation

We now consider the cleaved (010) surface (equivalent to the (001) plane in our $I2/b$ cell) terminated by fully-coordinated vanadium atoms and 6-fold coordinated bismuth atoms. As mentioned earlier, the (010) surface has one of the lowest calculated surface energies.^{32,65} Since epitaxial single-crystalline samples can be grown and single-crystalline samples can be cleaved along the (010) surface, we can make direct comparisons between our calculations and experiment. As mentioned in the Introduction, we use our single-crystalline epitaxial samples as a point of comparison and bridge between single-crystalline (ideal electrode) and polycrystalline samples (actual electrode used in devices).

Allowing our slab calculations to relax results in a (1x1) surface reconstruction, as shown in Figure 2(a) and (b), which agrees with low energy electron diffraction (LEED) measurements on single-crystalline samples.¹¹ In the first layer from the surface, the exposed V-O groups contract by $\sim 3.4\%$ for the bonds pointing towards the vacuum but elongate by $\sim 4.8\%$ for those pointing towards the bulk. A 2.2% elongation of the Bi-O bond length complements the relaxation for the bonds pointing towards the vacuum, with up to 6.1% contraction for bonds pointing towards the bulk. This is accompanied by a small increase in relative displacement along z between the V and Bi (on the order of 0.04 Å). In the second layer, the reverse occurs; that is, V-O bonds elongate by 2.5% for bonds pointing towards the vacuum but contract by 1.5% for bonds pointing towards the bulk. Conversely, the Bi-O bonds contract by 3.5% for bonds pointing to the vacuum and elongate by 1.9% for those pointing towards the bulk. By the third layer from the surface, the V-O and Bi-O have essentially returned to their bulk bond lengths. A histogram detailing the change in V-O and

Bi-O bond lengths is given in Figure 2(c). An important consequence of this relaxation in the (010) surface is the observation of facet-dependent accumulation of carriers as explained below.

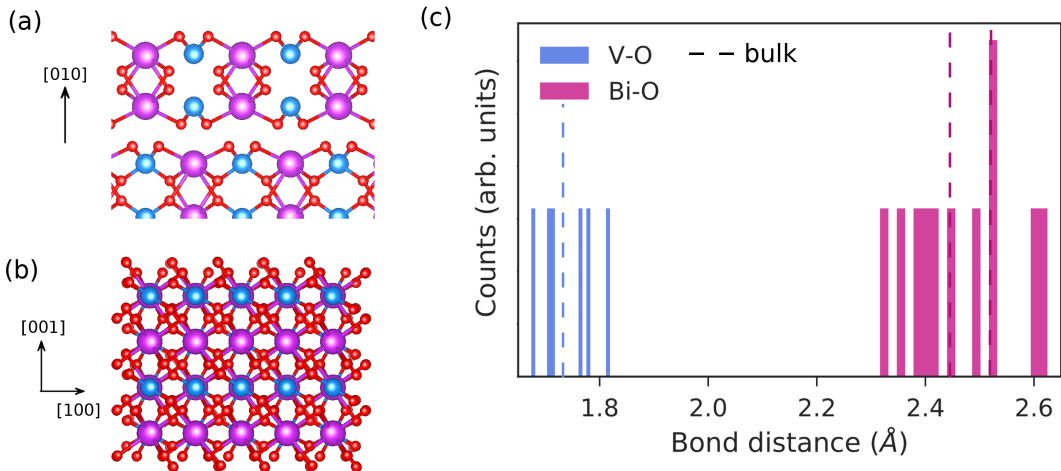


Figure 2: (a) Side and (b) top view of the relaxed (010) surface in BiVO₄. To illustrate the pattern of surface relaxations, only V-O bonds less than the bulk bond length of 1.74 Å and Bi-O bonds less than 2.55 Å are shown. (c) The corresponding histogram distribution of the V-O and Bi-O bond lengths within the first three layers of the surface; bulk bond lengths are shown as dashed lines.

In order to extract band edges and the work function, we align computed eigenvalues to the vacuum level using the electrostatic potential, which consists of the bare ion and Hartree potential. The electrostatic potential is averaged within the plane for each atomic layer to obtain the microscopic potential and then averaged again out of the plane to yield the macroscopic potential. An example is shown in Figure 3. As a result of the structural relaxation described previously, a potential well emerges in the average electrostatic potential \tilde{V} that results in an accumulation of electrons. A similar potential well feature occurs at the DDH level (see SI). This is consistent with experiments that suggest certain facets have preferential accumulation of electrons.^{41,42,66,67} For instance, deducing from the growth patterns of photo-deposition of dual precursors, Li et al.⁴² demonstrated that the {010} facet prefers reduction reactions, which suggests electron accumulation. Similarly, Tachikawa et al.⁶⁶ used potential-induced spatially-resolved photoluminescence emission to show other low-

index facets instead prefer hole accumulation. We discuss the impact of surface relaxation on the formation of small polarons in Section 6.

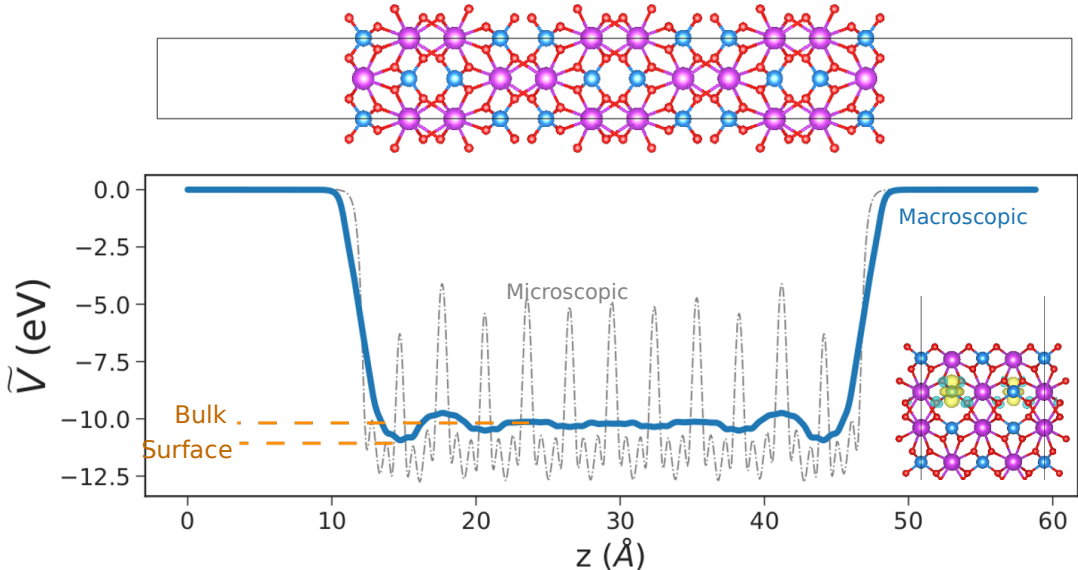


Figure 3: Microscopic and macroscopic average electrostatic potential \tilde{V} of the (010) slab obtained using DFT+U. The orange dashed lines indicate the potential at the surface and in the bulk averaged along the z direction. The surface \tilde{V} is 0.68 eV below that of the bulk. This potential leads to electron accumulation, as shown in charge density inset displaying the spin-polarization (defined as the difference in spin up and spin down charge densities, $\Delta\rho = \rho_{\text{up}} - \rho_{\text{down}}$; yellow is positive $\Delta\rho$ and blue is negative $\Delta\rho$) for an extra electron in the pristine slab.

5.2 Band alignment

Next we compare our slab calculations with band alignment measurements on previously reported single-crystalline samples from Ref. 11 to evaluate the accuracy of our structural models. Figure 4 shows a direct comparison between theory and experiment on the absolute position of the band edges with respect to vacuum, along with the standard hydrogen and oxygen redox potentials.

Similar to the band gap, there is a serendipitous agreement in band alignment between DFT+U at $T=0$ and experiment, with differences ~ 0.2 eV. Indeed, temperature renormalization plays an important role in the absolute position of the bands. We can make

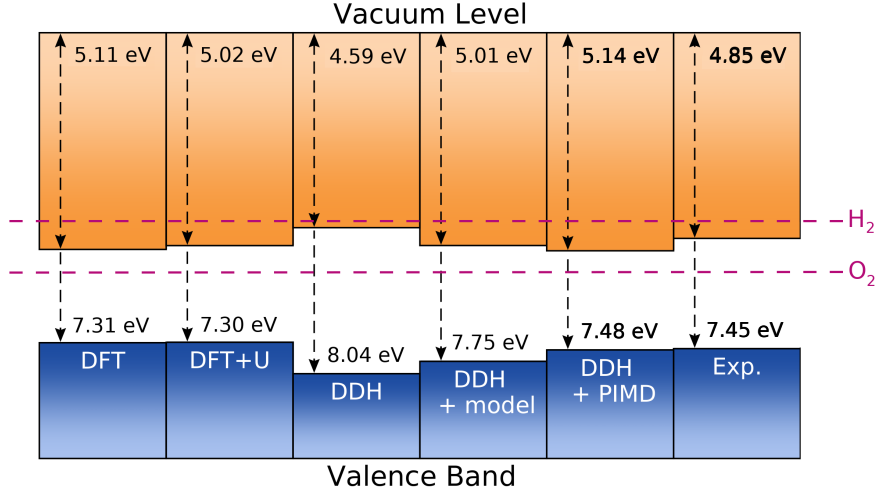


Figure 4: Band alignments for BiVO_4 at DFT, DFT+U, DDH⁵⁸ levels of theory as referenced to the vacuum. Two estimates for temperature renormalization are given: (DFT+model) based on the equations from Ref. 68 and (DFT+PIMD) from the results of Ref. 34. Single-crystalline experimental measurements are taken from Ref. 11. For convenience, the hydrogen and oxygen redox potentials are given as dotted lines. See text and SI for further details. Generated with `bapt`, <https://github.com/utf/bapt>.

two estimates on the effect of temperature, involving a rigid shift in the band edge using 1) values calculated with path-integral molecular dynamics (PIMD)³⁴ and 2) values based on Rayleigh-Schrödinger perturbation theory for electron-optical phonon interactions⁶⁸ (see SI for calculation details). Using a screened hydrogenic model, the exciton binding energy is estimated to be ~ 0.18 eV, which is a slight overestimate to the value derived from explicit calculations based on GW quasiparticle eigenvalue shifts (0.11 eV³⁴). Using method 1), the combined renormalization from nuclear quantum effects and finite temperature is $\Delta\text{VB} \approx 0.56$ and $\Delta\text{CB} \approx -0.36$ eV (using PBE0). Spin-orbit coupling leads to primarily a lowering of the conduction band states. Adding spin-orbit coupling and excitonic effects, we obtain $\Delta\text{VB} \approx 0.61$ and $\Delta\text{CB} \approx -0.54$ eV. For method 2), we estimate $\Delta\text{VB} \approx 0.29$ and $\Delta\text{CB} \approx -0.42$ eV, where spin-orbit coupling and the excitonic binding energy calculated from the hydrogenic model are included. As Figure 4 illustrates, when these corrections are included, the agreement between experiment and DDH improves whereas DFT+U at $T=0$ provides accidental agreement to the correct band alignment. Thus, a finite-temperature

study of interfacial and surface phenomena in BiVO_4 requires at minimum an hybrid functional level of theory to provide an accurate description. Studies on other oxides like WO_3 similarly find strong temperature renormalization effects.⁶⁹ Nevertheless, as demonstrated in Refs. 21 and 45, DFT+U qualitatively agrees with DDH calculations for explaining major trends in the electronic structure, formation energies, and polaron formation related to the oxygen vacancy. Thus, below we use DFT+U to characterize the substoichiometric surface, focusing on trends.

6 Substoichiometric (010) Surface

6.1 Formation of polarons

In general, the formation of an electron polaron involves the localization of an electron on an atomic site; in the case of BiVO_4 , the polaron self-traps on the vanadium sites, changing the nominal V^{5+} charge state to V^{4+} . We distinguish between three cases: 1) an extra electron is introduced in the pristine structure and it is delocalized instead of forming a polaron, 2) an extra electron is introduced in the pristine structure and it localizes to form a polaron, 3) an oxygen vacancy is introduced and the associated electron(s) localize nearby to form polarons. We define the polaron binding energy as the total energy difference between 1) and 2). The energy difference between the level in the band gap corresponding to 2) and defect charge-transition level of 3) is defined as the ionization energy of a defect polaron with respect to a polaron far from the defect. This is different from the ionization energy defined with respect to the conduction band minimum, and it is the former that is important to consider in studying polaron hopping. In Section 6.2, we further distinguish between polarons formed at the surface and in the bulk.

We first note that when an extra electron is introduced to the pristine surface, it can be stabilized as a polaron, as in the case of an extra electron introduced in the bulk.³⁷ We calculated the polaron binding energy to be 0.12 eV for the surface, compared to 0.52 eV in

the bulk.¹⁴ This suggests that electron polarons tend to occur in the pristine bulk rather than the pristine surface. Wiktor et al.^{36,37} similarly find the surface polaron has a 0.4 eV smaller binding energy compared to the bulk polaron for the pristine bulk and pristine surface at finite temperature (0.18 eV smaller in the presence of water).

Next, we introduced oxygen vacancies and we present a comparison of the oxygen vacancy formed in the bulk²¹ and at the surface and of the accompanying formation of small polarons. We calculated surface polaron configurations analogous to those in the bulk (see Ref. 21), adopting similar naming conventions. Electron polaron formation in BiVO₄ is accompanied by an expansion of V-O bond lengths. At the surface, this is as much as 4.4%. Figure 5 presents the spin-polarized charge densities of each of these configurations and their relative stabilities for the neutral oxygen vacancy where two excess electrons are left behind. For each configuration, we initialize the relaxed pristine surface structure to favor polaron formation at a specific V site through 1) inducing a slight expansion ($\sim 3\%$) of V-O bond lengths and 2) inducing a finite magnetic moment in the spin-up configuration at specified sites; then, we label these configurations by C1 through C6 and allow each configuration to relax. Configurations C1-C4 involve localization of electrons on the VO₃ polyhedron containing the defect site. In configurations C2-C6, the structure is modified in such a way that the VO₃ polyhedron shares an oxygen of a neighboring VO₄ one layer below the exposed surface. In other possible configurations, C3, C5, and C6 involve localization on either a neighboring corner-sharing VO₄ or a VO₄ in the proximity.

Each of these configurations were triplet states (S=1); as in the bulk, the triplet is slightly more stable than the singlet (by about 30.7 meV at the surface using DFT+U). At the surface, configurations where the VO₃ polyhedron distorts to share an O corner with a neighboring VO₄ tetrahedron are energetically favored, much like in the bulk. The lowest polaron formation C5 is favored by approximately 650 meV compared to C1, which is markedly smaller than the largest relative energy differences in the bulk (nearly 800 meV). In general, a self-trapped electron is accompanied by a local expansion of the lattice, in this

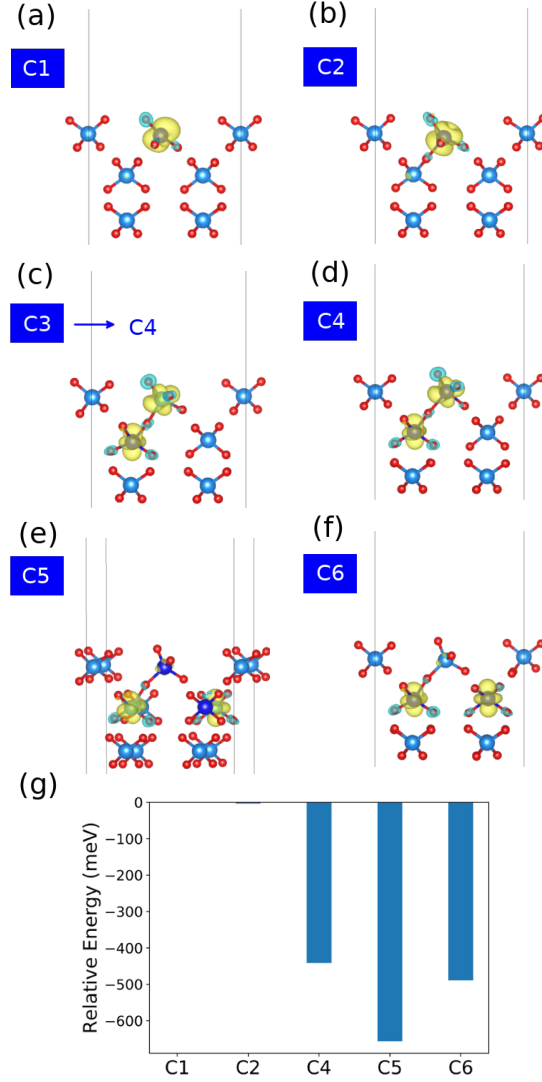


Figure 5: Possible configurations for small polaron formation near an oxygen vacancy V_O at the (010) surface of BiVO_4 (a-f) and (g) corresponding relative total energies with respect to the first configuration (C1) obtained using DFT+U. Bi atoms are omitted for clarity. Oxygen atoms are represented in red; V atoms are blue and darker colored V indicate sites of initial polaron formation before relaxation. The spin-polarization (defined as the difference in spin up and spin down charge densities, $\Delta\rho = \rho_{\text{up}} - \rho_{\text{down}}$) of the relaxed structure is shown in yellow (positive $\Delta\rho$) and blue (negative $\Delta\rho$). (a) Two electrons donated by the V_O localize entirely at the defect site at the surface. (b-f) The VO_3 polyhedron containing the V_O shares an O with a neighboring VO_4 . (b) Both electrons localize at defect site. (c) Both electrons initialized to localize on a corner-sharing VO_4 , but relaxes to C4. (d) Each electron localizes on the surface VO_3 and a corner-sharing VO_4 . (e) Despite being configured towards charge localization on the VO_3 polyhedron and a neighboring VO_4 , the relaxed configuration results in polarons on the corner-sharing VO_4 and a separate VO_4 . (f) An electron localizes at the corner-sharing VO_4 and a separate VO_4 near the surface.

case the V-O bonds in a vanadium-centered polyhedron. The formation of a surface polaron must thus compete with existing surface relaxations consisting of alternating bond length contractions and elongations, as described in Section 5.1, and thus leads to a higher energetic cost in lattice strain. Hence, the surface polaron in the presence of an oxygen vacancy tends to form in the second layer from the surface where surface relaxations are smaller (e.g., C4 through C6). Nevertheless, the formation of electron polarons near the oxygen vacancy is favorable at the surface, as it is in the bulk.

6.2 Defect Formation Energies

Oxygen vacancies are n -type defects that in principle can take on 0, 1+, or 2+ charge states. In order to understand the thermodynamic stability of forming an oxygen vacancy, we calculate the formation energy and compare it with the corresponding one in the bulk. This comparison is shown as Figure 6 at the DFT+U level. In the bulk,²¹ the oxygen vacancy can take on +2, +1, and neutral charge states. The charge-transition level (CTL) for (+1/2+) is reported to be 0.87 eV and for (1+/0) as 0.59 eV below the conduction band minimum (CBM).²¹ Thus, the oxygen vacancy in the bulk is a deep donor with an ionization energy of 0.59 eV with respect to the conduction band minimum. However, the ionization energy with respect to a small polaron in the pristine bulk away from the oxygen vacancy is on the order of 0.21 eV (at DDH it is 0.11 eV). At finite temperature, this energy difference is expected to be small enough so that the polaron formed from oxygen vacancies in the bulk can contribute to conductivity via polaron hopping. This is consistent with experimental measurements on mobility that indicate thermally activated small polaron hopping to be the dominant conduction mechanism at room temperature (at lower temperatures variable polaron hopping is reported as the dominant contributor to conductivity instead).^{25,70}

In contrast, the surface oxygen vacancy is predominantly stable as the +1 and neutral charge states for most values of the Fermi level in the band gap. The fact that the +2 charge state is found to be less stable at the surface than in the bulk may be related to surface

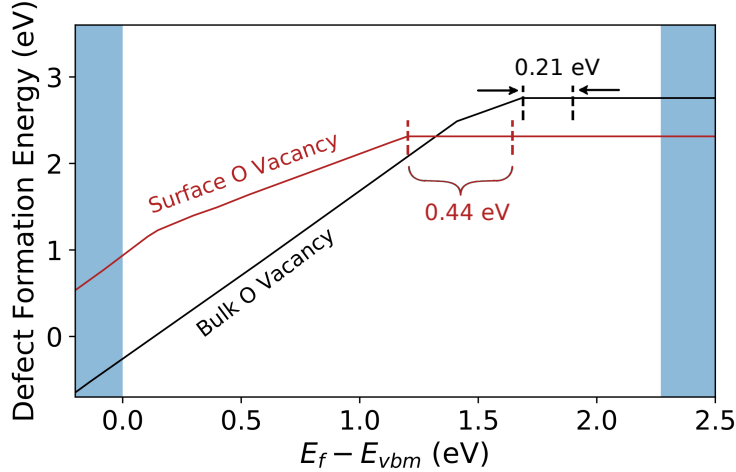


Figure 6: Comparison of defect formation energies of the surface and bulk oxygen vacancy under oxygen-rich conditions as a function of the Fermi level E_f position obtained using DFT+U. The slope of each curve corresponds to the charge state of the defect with intersections corresponding to charge-transition levels (CTL). These curves represent the lowest energy configuration. The band edges are shown with shaded blue areas. The black dotted lines indicate energy difference between the (+1/0) CTL and the polaron level in bulk BiVO_4 , i.e., the ionization energy of the neutral oxygen vacancy to polaron level is 0.21 eV. That difference is 0.44 eV between the neutral surface oxygen vacancy CTL and surface polaron level, as indicated by the red dotted lines. Bulk oxygen vacancy formation energies are from Ref. 21.

relaxations, which tend to create a potential well that attracts electrons, as discussed in Section 5.1. The (1+/0) CTL for the surface defect is significantly deeper than that in the bulk, at 1.07 eV below the CBM, indicating that the neutral oxygen vacancy is the dominant charge state for most values of interest for the Fermi level position. As with the bulk, we calculated the difference between the (+1/0) CTL to the level associated with an electron polaron at the pristine surface, and find an energy difference of 0.44 eV. Even at finite temperature (e.g., ambient conditions), this barrier would be unfavorable for polaron hopping compared to the bulk; thus, we do not expect surface polarons from oxygen vacancies to contribute significantly to mobility.

We note that our calculated formation energies are up to 1 eV smaller than those reported in Ref. 45, which may be due to their use of the PBEsol functional as well as different choices of the simulation cell. Hegner et al⁴⁵ use a 6-layer slab (compared to our 8-layer slab),

which exhibits uneven relaxation and has no effective bulk region, as surface relaxations occur throughout the slab. For the tetragonal structures relaxed with PBEsol, the in-plane lattice parameters are $a = 5.117$ and $c = 11.587 \text{ \AA}$.⁴⁵ Our calculated lattice parameters for the tetragonal cell with PBE+U are $a = 5.172$ and $c = 11.770 \text{ \AA}$. We note that our lattice parameters are in better agreement with measured BiVO₄ lattice parameters (see comparison with experiment in Table S3 of SI) and hence the local bonding environment, which plays an important role in charge localization.

7 Variation of work function with oxygen vacancy concentration

We next calculate the variation of the work function φ with oxygen vacancy concentration and compare with experiment. Oxygen atoms are removed from each exposed surface within the first two layers from the surface in incremental amounts. Effectively this amounts to removing two oxygen atoms per 1 at% in our $2 \times 2 \times 2$ 192-atom supercell (where at% is defined with respect to the total number of atoms). Table 1 lists our calculated work function φ as a function of oxygen vacancy. The corresponding density of states are presented in the SI. Not surprisingly for an n -type defect, a higher oxygen vacancy concentration results in a lower work function (i.e., higher Fermi level). Overall, our calculations suggest the work function can decrease up to 0.7 eV for up to 5 at% oxygen vacancy concentration.

We next compare our calculated work function values with those in the literature. We note that our calculated work functions are lower by up to 1 eV compared to other computational studies.^{41,45} We find that a higher calculated work function can arise from a poorer sampling of the Brillouin zone in the calculation of the density of states from which the Fermi level is determined. Our work functions are calculated to within 0.02 eV computational accuracy with respect to k -point sampling; further details are provided in the SI, including comparison with literature values. When comparing with measured work functions (e.g., as

done in Ref. 45), we note that caution must be taken, as the work function can be highly sensitive to surface features, surface defects, and surface contaminants.^{12,71,72} For example, Hermans et al^{71,72} deposited polycrystalline BiVO₄ thin films interfaced with various oxides using pulsed laser deposition and measured work functions that range between 5.6 eV to 6.6 eV. In another study, Cooper et al¹² grew polycrystalline thin films with chemical vapor deposition and measured a work function of 5.27 eV. These studies illustrate the sensitivity of work functions to polycrystallinity, sample preparation procedure, and surface and/or interfacial effects. Hence, because of differences in sample preparation and unclear sample stoichiometries, it is challenging and delicate to make a one-to-one comparison between calculated and measured work functions.

Here, in order to validate the level of theory we used to calculate the work function, we compare with the measured work function reported in Ref. 11, where Czolchralski-grown stoichiometric single-crystalline samples were used. These measurements remove any uncertainties introduced by polycrystallinity or interfacial effects. Furthermore, the level of surface contaminants was found to be below detectable levels in x-ray photoelectron spectroscopy measurements. Since undoped single-crystalline samples are too insulating for reliable measurements, ~ 1 at% Mo-doping was used to improve sample conductivity. The measured relative stoichiometry was reported to be Mo_{0.02}:Bi_{1.09}V_{1.00}O_{4.04}, which is within the nominal 1 at% Mo-doping stoichiometry of Mo_{0.06}:Bi_{1.00}V_{1.00}O_{4.00} when considering instrument detection limits.¹¹ Favaro et al¹¹ measured a work function of 5.15 eV. In order to better compare with this sample, we calculate the work function with 1 at% Mo-doping. Our calculations suggest that 1 at% Mo-doping can lead to comparable decreases in the work function as that of 1 at% oxygen vacancies ($\varphi \sim 4.9$ eV). The measured work function of 5.15 eV is within the range of our calculated work functions for the pristine and 1 at% Mo-doped slabs (5.40 eV and 4.86 eV, respectively). The fact that the measured work function is somewhat larger than the calculated work function for 1 at% Mo-doping is reasonable considering that the measured stoichiometry has a smaller Mo concentration compared to the nominal

stoichiometry. This agreement further validates our structural model and methodology.

Table 1: Calculated work function φ for Mo-doping and various concentrations of oxygen vacancies using DFT+U. Labels correspond to the number of defects present per exposed surface; each removed oxygen or substituted Mo corresponds to 1 at%.

Config.	φ (eV)
pristine	5.401
1 Mo _V	4.906
1 V _O	4.861
5 V _O	4.670

Next, in order to validate whether our calculated work function as a function of surface oxygen vacancy concentration on the (010) surface is reasonable, we measured the work function of the (010) plane of epitaxially-grown single-crystalline samples. The surface of these samples is expected to be well defined and significantly more uniform than typical polycrystalline samples having randomly oriented grains with varying defect levels. Thus, this sample is appropriate to validate our calculations. The work function of this sample was determined using ultraviolet photoemission spectroscopy (UPS). Further details on the experimental set up and analysis procedure for accurately measuring the work function are provided in the SI.

The surface oxygen vacancy concentration on the (010) plane of the epitaxially-grown single crystalline samples were determined by quantitative analysis of the V $2p_{3/2}$ peaks of the x-ray photoelectron spectra, which is sensitive only to the surface composition. Ideally on average, each oxygen vacancy reduces two V⁵⁺ to two V⁴⁺ when there are no other dopants that affect the oxidation states of V. Therefore, the surface oxygen vacancy concentration can be reasonably estimated by quantifying the fraction of V that is present as V⁴⁺. From a previously reported study that used samples prepared in the same way as ours,²⁷ the percent concentration of V⁴⁺ ($\equiv \%V^{4+} = V^{4+}/(V^{4+} + V^{5+}) \times 100$) of the epitaxially-grown single crystalline sample was determined to have a $\%V^{4+}$ of 3.7%. This is equivalent to ~ 0.6 at% (with respect to total number of atoms), meaning that the surface oxygen vacancy concentration of the epitaxially-grown single-crystalline sample is ~ 0.3 at%. The measured

work function for undoped BiVO_4 with 0.3 at% oxygen vacancies (4.94 eV) is within the range between the calculated work function for the pristine (5.40 eV) and 1 at% oxygen vacancy concentration (4.86 eV). These comparisons demonstrate that our calculations are able to capture the change in the work function in the presence of oxygen vacancies. To our knowledge, this is one of the first direct comparisons between calculations and measurements on single-crystalline samples with well-defined surfaces and quantified composition (in stoichiometry or estimated % V^{4+}).

8 Discussion

We now discuss the different behaviors of the bulk and surface polarons that arise from the presence of oxygen vacancies in BiVO_4 . Based on an analysis of single-particle energies, Wiktor et al.³⁶ report that holes tend to localize at the *pristine* surface (i.e., without oxygen vacancies) and electron polarons tend to be stable in the pristine bulk, thus hinting at a robust charge separation mechanism. Our study of the *defective* surface with oxygen vacancies illustrates that the presence of oxygen vacancies leads to localization of electrons in various configurations, which may therefore promote charge recombination at the surface. For the (010) surface termination that favors electron accumulation, we find that these electrons form small polarons that tend to remain localized and immobile around the defect site. Using a combination of DFT+U and hybrid functional calculations, Hegner et al.⁴⁵ proposed a picture similar to ours, where oxygen migration in the bulk faces moderate (0.2-0.4 eV) energy barriers and thus may lead to increased ionic and consequently electronic conductivity; in contrast, migration at the surface has large (~ 1 eV) energy barriers to ionic (and consequently electronic) migration and are thus immobile. In addition to the neutral charge state considered in Ref. 45, we considered the 1+ and 2+ charge states of the oxygen vacancy. Furthermore, the ionic migration reported in Hegner et al is only part of the picture; that is, the energy barrier to polaron hopping (without any ionic migration) is small

enough in the bulk for polarons to contribute to mobility via polaron hopping but is less favorable for the surface polaron near an oxygen vacancy. Rossell et al.⁷³ reported surface reduction of V sites using electron energy loss spectroscopy in combination with scanning transmission electron microscopy and interpreted this as segregation of oxygen vacancies at the surface, which is consistent with our observation of surface polarons accumulating in the presence of surface defects. Consistently, using differential absorption spectroscopy, Selim et al. suggested that the change in conductivity with moderate thermal heating arises from de-trapping oxygen vacancies.⁴⁴ In fact they report the ionization energy of V^{4+} to V^{5+} to be ~ 0.2 eV, in close agreement with bulk oxygen vacancy ionization energy reported in Ref. 21, further confirming that our methodology and the chosen level of theory are appropriate.

We note that our characterization of the surface oxygen vacancy is at 0 K and referenced to the vacuum. As with band alignments, we anticipate temperature corrections (and separately solvation effects) to play a critical role in the electronic behavior of these defects. Ref. 37 reported a reduction in electron polaron binding energies at finite temperature on the order of 200 meV for bulk polarons; a similar effect may occur for surface polarons. The pattern of surface relaxation at 0 K described in Section 5.1 also occurs at finite temperature,³⁶ as this minimizes dangling bonds and is energetically favorable. Thus we would anticipate there would likewise be a tendency for electron accumulation at the surface. Another anticipated effect is temperature fluctuations in band edges, as in the case of WO_3 , which has on average fluctuations of 0.3 eV at 300 K.⁶⁹ $BiVO_4$ and WO_3 have comparable dielectric constants and longitudinal optical phonon frequencies ($BiVO_4$: $\epsilon_\infty = 6.9$,¹⁴ $\omega_{LO} = 828$ cm^{-1} ,^{72,74} WO_3 : $\epsilon_\infty = 4.5$,⁶⁹ $\omega_{LO} = 842$ cm^{-1} ⁷⁵), and therefore comparable electron-phonon coupling strengths may be expected. Thus, we anticipate comparable band edge fluctuations at ambient conditions for $BiVO_4$.

Ultimately, in addition to temperature, the interface with water will heavily determine the reactivity for water splitting for which surface defects will play an important role. When used without any oxygen evolution catalyst, $BiVO_4$ has relatively low photocurrent densities

and its photocurrent onset is shifted towards the positive direction because its surface is not catalytic for water oxidation.^{76,77} The resulting surface accumulated holes can lead to surface recombination and/or photocorrosion.⁷⁶ Whether the surface electron polaron plays an active, indirect, or passive role in charge transfer reactions and the overall reaction of water oxidation depends critically on the nature of the interface. Therefore, a further study is necessary to investigate how the surface oxygen vacancies and polaron formation are affected when the surface of BiVO₄ is in contact with water and with oxygen evolution catalysts in order to understand the overall photoelectrochemical properties of the this oxide system.

Overall, our findings suggest the following implications of oxygen vacancies to photoelectrochemical performance. First, surface polarons derived from oxygen vacancies are expected to contribute little to the overall mobility of electrons in BiVO₄ as a photoanode. Second, such electron polarons may act as recombination centers for holes shuttled towards the (010) surface during water oxidation if the interfacial hole transfer for oxygen evolution is slow. Third, the tendency to form small polarons at the surface will have a large impact on the interaction of the BiVO₄ surface with the oxygen evolution catalyst and interfacial water, and may significantly affect the interfacial charge transfer and/or recombination. Thus, it is critical when comparing theory and experiment to have a thorough characterization of surface defects. We expect water adsorption, surface terminations, and the addition of the oxygen evolution catalyst to heavily interact with surface defects and play an important role in the overall performance of BiVO₄ as a photoanode. Work is in progress to construct a holistic understanding of interfacial properties of BiVO₄.

9 Conclusions

In conclusion, we presented a systematic study of the (010) surface in BiVO₄ with and without oxygen vacancies using first-principles calculations and compared them with experimental measurements. First, we benchmarked DFT, DFT+U and hybrid functionals for the

bulk and pristine surface, comparing lattice parameters and band gaps, and showed hybrids are the minimum level of theory needed to describe the band alignment. We validated our structural model and level of theory for slab calculations; our calculated band alignment and work function show excellent agreement with measurements obtained from single-crystalline samples when thermal renormalization, exciton effects, and spin-orbit coupling are taken into account. With an accurate model of the pristine surface, we next investigate the influence of surface reconstructions. While the (1x1) surface reconstruction results in minimal in-plane structural relaxation, the out-of-plane relaxations lead to an alternating pattern of contracted and elongated Bi-O and V-O bonds within the first two layers of the surface. For the (010) surface, this pattern of relaxation leads to a potential well for which electron accumulation is expected.

Such an electron accumulation is closely related to the formation of oxygen vacancies and small polarons. Similar to the bulk, surface polarons may form at a pristine or substoichiometric surface. Although polaron configurations analogous to the bulk are stable at the surface, the difference in relative stabilities of various configurations is smaller (by around 0.15 eV) than in the bulk. We attribute this difference to the fact that polaron formation is accompanied by a local lattice expansion that competes with surface relaxations.

To explore the thermodynamic stability and charge transition levels (CTLs) of possible charge states for the oxygen vacancy, we calculated the defect formation energy diagram. For both the bulk and surface, the oxygen vacancy is found to be a deep donor. In contrast to the bulk oxygen vacancies, the surface polaron is a much deeper donor (relative to the conduction band minimum) and also energetically far from the surface or bulk polaron level of a pristine slab. This indicates that while bulk polarons may contribute to mobility, surface polarons likely do not.

Finally, we performed a study of the variation of the work function in BiVO_4 with oxygen vacancy concentration. We found good agreement between measured single-crystalline samples and calculated values for the defect-free, pristine structure. More importantly, we

showed that our calculations capture and quantify the change in work function in the presence of oxygen vacancies in epitaxially-grown single-crystalline samples. This consequently confirms the validity of our structural model and will allow for more meaningful comparison and conclusions when studying properties of polycrystalline BiVO_4 in photoelectrochemical devices.

Overall, our study showed that 1) hybrid functionals are needed to accurately capture band alignment, 2) while the role of oxygen vacancies at the surface may be beneficial in some aspects (e.g., adsorption), its tendency for charge localization may be harmful to conductivity and lead to recombination centers that consume holes needed for water oxidation, and 3) defects in the bulk and at the surface behave differently and their different behavior must be taken into account to understand the photoelectrochemical behavior of BiVO_4 . We expect surface oxygen vacancies to play a critical and diverse role in water splitting reactions, particularly in charge transfer mechanisms when coupled with the oxygen evolution catalyst and when interfaced with water. Our study lays the groundwork for understanding electronic behavior and polaron formation of surface oxygen vacancies in BiVO_4 , and overall for other catalytic metal oxides.

Acknowledgements

The authors thank David Starr and Marco Favaro for fruitful discussions on single crystalline measurements. This material is based upon work supported by the National Science Foundation (NSF) under Grant No. CHE-1764399. Part of this research used resources of the Center for Functional Nanomaterials, which is a U.S. DOE Office of Science User Facility, at Brookhaven National Laboratory under Contract No. DE-SC0012704. P.S. and J.K. are supported by the Army Research Office (W911NF-17-1-0254) and NSF CAREER (DMR-1752797). This work was completed in part with resources provided by the University of Chicago's Research Computing Center.

Supporting Information Available

The following files are available free of charge: bvo-surf-supplementary.pdf: procedure for photoemission spectroscopy measurements and work function determination, comparison of \tilde{V} with DDH, convergence of slab calculations, charge state corrections, determination of work function and Fermi level, pristine bulk and surface structural and electronic parameters, determination of chemical potential in defect formation energies

Input files, structure files, and scripts for generating the data in the main text and SI are available on QRESP (www.qresp.org), an open-source curation and exploration software for reproducibility in scientific research.

References

- (1) Nozik, A. J. Photoelectrochemistry: Applications to Solar Energy Conversion. Annual Review of Physical Chemistry **1978**, 29, 189–222.
- (2) Grätzel, M. Photoelectrochemical Cells. Nature **2001**, 414, 338–344.
- (3) Turner, J. A. Sustainable Hydrogen Production. Science **2004**, 305, 972–974.
- (4) Walter, M. G.; Warren, E. L.; McKone, J. R.; Boettcher, S. W.; Mi, Q.; Santori, E. A.; Lewis, N. S. Solar Water Splitting Cells. Chemical Reviews **2010**, 110, 6446–6473.
- (5) McKone, J. R.; Lewis, N. S.; Gray, H. B. Will Solar-Driven Water-Splitting Devices See the Light of Day? Chemistry of Materials **2014**, 26, 407–414.
- (6) Lewis, N. S. Introduction: Solar Energy Conversion. Chemical Reviews **2015**, 115, 12631–12632.
- (7) Chu, S.; Li, W.; Yan, Y.; Hamann, T.; Shih, I.; Wang, D.; Mi, Z. Roadmap on Solar Water Splitting: Current Status and Future Prospects. Nano Futures **2017**, 1, 022001.

- (8) Zhu, S.; Wang, D. Photocatalysis: Basic Principles, Diverse Forms of Implementations and Emerging Scientific Opportunities. Advanced Energy Materials **2017**, 7, 1700841.
- (9) Park, Y.; McDonald, K. J.; Choi, K.-S. Progress in Bismuth Vanadate Photoanodes for Use in Solar Water Oxidation. Chem. Soc. Rev. **2013**, 42, 2321–2337.
- (10) Kim, T. W.; Choi, K.-S. Nanoporous BiVO₄ Photoanodes with Dual-Layer Oxygen Evolution Catalysts for Solar Water Splitting. Science **2014**, 343, 990–994.
- (11) Favaro, M.; Uecker, R.; Nappini, S.; Piš, I.; Magnano, E.; Bluhm, H.; van de Krol, R.; Starr, D. E. Chemical, Structural, and Electronic Characterization of the (010) Surface of Single Crystalline Bismuth Vanadate. The Journal of Physical Chemistry C **2019**, 123, 8347–8359.
- (12) Cooper, J. K.; Gul, S.; Toma, F. M.; Chen, L.; Glans, P.-A.; Guo, J.; Ager, J. W.; Yano, J.; Sharp, I. D. Electronic Structure of Monoclinic BiVO₄. Chemistry of Materials **2014**, 26, 5365–5373.
- (13) Kudo, A.; Omori, K.; Kato, H. A Novel Aqueous Process for Preparation of Crystal Form-Controlled and Highly Crystalline BiVO₄ Powder from Layered Vanadates at Room Temperature and Its Photocatalytic and Photophysical Properties. Journal of the American Chemical Society **1999**, 121, 11459–11467.
- (14) Kim, T. W.; Ping, Y.; Galli, G. A.; Choi, K.-S. Simultaneous Enhancements in Photon Absorption and Charge Transport of Bismuth Vanadate Photoanodes for Solar Water Splitting. Nature Communications **2015**, 6, 8769.
- (15) Malashchonak, M. V.; Streltsov, E. A.; Kuliomin, D. A.; Kulak, A. I.; Mazanik, A. V. Monoclinic Bismuth Vanadate Band Gap Determination by Photoelectrochemical Spectroscopy. Materials Chemistry and Physics **2017**, 201, 189–193.

- (16) Payne, D. J.; Robinson, M. D. M.; Egdell, R. G.; Walsh, A.; McNulty, J.; Smith, K. E.; Piper, L. F. J. The Nature of Electron Lone Pairs in BiVO₄. Applied Physics Letters **2011**, 98, 212110.
- (17) Murphy, A.; Barnes, P.; Randeniya, L.; Plumb, I.; Grey, I.; Horne, M.; Glasscock, J. Efficiency of Solar Water Splitting Using Semiconductor Electrodes. International Journal of Hydrogen Energy **2006**, 31, 1999–2017.
- (18) Kim, J. H.; Jang, J.-W.; Jo, Y. H.; Abdi, F. F.; Lee, Y. H.; van de Krol, R.; Lee, J. S. Hetero-Type Dual Photoanodes for Unbiased Solar Water Splitting with Extended Light Harvesting. Nature Communications **2016**, 7, 13380.
- (19) Tolod, K. R.; Hernández, S.; Russo, N.; Tolod, K. R.; Hernández, S.; Russo, N. Recent Advances in the BiVO₄ Photocatalyst for Sun-Driven Water Oxidation: Top-Performing Photoanodes and Scale-Up Challenges. Catalysts **2017**, 7, 13.
- (20) Cooper, J. K.; Scott, S. B.; Ling, Y.; Yang, J.; Hao, S.; Li, Y.; Toma, F. M.; Stutzmann, M.; Lakshmi, K. V.; Sharp, I. D. Role of Hydrogen in Defining the N-Type Character of BiVO₄ Photoanodes. Chemistry of Materials **2016**, 28, 5761–5771.
- (21) Seo, H.; Ping, Y.; Galli, G. Role of Point Defects in Enhancing Conductivity of BiVO₄. Chemistry of Materials **2018**, 30, 7793–7802.
- (22) Zhao, X.; Hu, J.; Yao, X.; Chen, S.; Chen, Z. Clarifying the Roles of Oxygen Vacancy in W-Doped BiVO₄ for Solar Water Splitting. ACS Applied Energy Materials **2018**, 1, 3410–3419.
- (23) Zhao, Z.; Luo, W.; Li, Z.; Zou, Z. Density Functional Theory Study of Doping Effects in Monoclinic Clinobisvanite BiVO₄. Physics Letters A **2010**, 374, 4919–4927.
- (24) Zhang, J.; Deng, M.; Ren, F.; Wu, Y.; Wang, Y. Effects of Mo/W Codoping on the

- Visible-Light Photocatalytic Activity of Monoclinic BiVO₄ within the GGA+U Framework. RSC Advances **2016**, 6, 12290–12297.
- (25) Rettie, A. J. E.; Lee, H. C.; Marshall, L. G.; Lin, J.-F.; Capan, C.; Lindemuth, J.; McCloy, J. S.; Zhou, J.; Bard, A. J.; Mullins, C. B. Combined Charge Carrier Transport and Photoelectrochemical Characterization of BiVO₄ Single Crystals: Intrinsic Behavior of a Complex Metal Oxide. Journal of the American Chemical Society **2013**, 135, 11389–11396.
- (26) Kweon, K. E.; Hwang, G. S.; Kim, J.; Kim, S.; Kim, S. Electron Small Polarons and Their Transport in Bismuth Vanadate: A First Principles Study. Physical Chemistry Chemical Physics **2015**, 17, 256–260.
- (27) Zhang, W.; Wu, F.; Li, J.; Yan, D.; Tao, J.; Ping, Y.; Liu, M. Unconventional Relation between Charge Transport and Photocurrent via Boosting Small Polaron Hopping for Photoelectrochemical Water Splitting. ACS Energy Letters **2018**, 3, 2232–2239.
- (28) Zhang, W.; Yan, D.; Li, J.; Wu, Q.; Cen, J.; Zhang, L.; Orlov, A.; Xin, H.; Tao, J.; Liu, M. Anomalous Conductivity Tailored by Domain-Boundary Transport in Crystalline Bismuth Vanadate Photoanodes. Chemistry of Materials **2018**, 30, 1677–1685.
- (29) Qiu, W.; Xiao, S.; Ke, J.; Wang, Z.; Tang, S.; Zhang, K.; Qian, W.; Huang, Y.; Huang, D.; Tong, Y.; Yang, S. Freeing the Polarons to Facilitate Charge Transport in BiVO₄ from Oxygen Vacancies with an Oxidative 2D Precursor. Angewandte Chemie International Edition **2019**, DOI: 10.1002/anie.201912475.
- (30) Zhang, W.; Song, L.; Cen, J.; Liu, M. Mechanistic Insights into Defect-Assisted Carrier Transport in Bismuth Vanadate Photoanodes. The Journal of Physical Chemistry C **2019**, 123, 20730–20736.
- (31) Walsh, A.; Yan, Y.; Huda, M. N.; Al-Jassim, M. M.; Wei, S.-H. Band Edge Electronic

- Structure of BiVO₄ : Elucidating the Role of the Bi s and V d Orbitals. Chemistry of Materials **2009**, 21, 547–551.
- (32) Zhao, Z.; Li, Z.; Zou, Z. Electronic Structure and Optical Properties of Monoclinic Clinobisvanite BiVO₄. Physical Chemistry Chemical Physics **2011**, 13, 4746–4753.
- (33) Ding, K.; Chen, B.; Li, Y.; Zhang, Y.; Chen, Z. Comparative Density Functional Theory Study on the Electronic and Optical Properties of BiMO₄ (M = V, Nb, Ta). Journal of Materials Chemistry A **2014**, 2, 8294.
- (34) Wiktor, J.; Reshetnyak, I.; Ambrosio, F.; Pasquarello, A. Comprehensive Modeling of the Band Gap and Absorption Spectrum of BiVO₄. Physical Review Materials **2017**, 1.
- (35) Wu, F.; Ping, Y. Combining Landau–Zener Theory and Kinetic Monte Carlo Sampling for Small Polaron Mobility of Doped BiVO₄ from First-Principles. Journal of Materials Chemistry A **2018**, 6, 20025–20036.
- (36) Wiktor, J.; Pasquarello, A. Electron and Hole Polarons at the BiVO₄–Water Interface. ACS Applied Materials & Interfaces **2019**, 11, 18423–18426.
- (37) Wiktor, J.; Ambrosio, F.; Pasquarello, A. Role of Polarons in Water Splitting: The Case of BiVO₄. ACS Energy Letters **2018**, 3, 1693–1697.
- (38) Wang, G.; Ling, Y.; Lu, X.; Qian, F.; Tong, Y.; Zhang, J. Z.; Lordi, V.; Rocha Leao, C.; Li, Y. Computational and Photoelectrochemical Study of Hydrogenated Bismuth Vanadate. The Journal of Physical Chemistry C **2013**, 117, 10957–10964.
- (39) Yin, W.-J.; Wei, S.-H.; Al-Jassim, M. M.; Turner, J.; Yan, Y. Doping Properties of Monoclinic BiVO₄ Studied by First-Principles Density-Functional Theory. Physical Review B **2011**, 83, 115102.

- (40) Wang, D.; Jiang, H.; Zong, X.; Xu, Q.; Ma, Y.; Li, G.; Li, C. Crystal Facet Dependence of Water Oxidation on BiVO₄ Sheets under Visible Light Irradiation. Chemistry – A European Journal **2011**, 17, 1275–1282.
- (41) Hu, J.; Chen, W.; Zhao, X.; Su, H.; Chen, Z. Anisotropic Electronic Characteristics, Adsorption, and Stability of Low-Index BiVO₄ Surfaces for Photoelectrochemical Applications. ACS Applied Materials & Interfaces **2018**, 10, 5475–5484.
- (42) Li, R.; Zhang, F.; Wang, D.; Yang, J.; Li, M.; Zhu, J.; Zhou, X.; Han, H.; Li, C. Spatial Separation of Photogenerated Electrons and Holes among {010} and {110} Crystal Facets of BiVO₄. Nature Communications **2013**, 4, 1432.
- (43) Hu, J.; Zhao, X.; Chen, W.; Su, H.; Chen, Z. Theoretical Insight into the Mechanism of Photoelectrochemical Oxygen Evolution Reaction on BiVO₄ Anode with Oxygen Vacancy. The Journal of Physical Chemistry C **2017**, 121, 18702–18709.
- (44) Selim, S.; Pastor, E.; García-Tecedor, M.; Morris, M. R.; Francas, L.; Sachs, M.; Moss, B.; Corby, S.; Mesa, C. A.; Gimenez, S.; Kafizas, A.; Bakulin, A. A.; Durrant, J. R. Impact of Oxygen Vacancy Occupancy on Charge Carrier Dynamics in BiVO₄ Photoanodes. Journal of the American Chemical Society **2019**, DOI: 10.1021/jacs.9b09056.
- (45) Hegner, F. S.; Forrer, D.; Galán-Mascarós, J. R.; López, N.; Selloni, A. Versatile Nature of Oxygen Vacancies in Bismuth Vanadate Bulk and (001) Surface. The Journal of Physical Chemistry Letters **2019**, 10, 6672–6678.
- (46) Yang, J.; Wang, D.; Zhou, X.; Li, C. A Theoretical Study on the Mechanism of Photocatalytic Oxygen Evolution on BiVO₄ in Aqueous Solution. Chemistry - A European Journal **2013**, 19, 1320–1326.
- (47) Oshikiri, M.; Boero, M. Water Molecule Adsorption Properties on the BiVO₄ (100) Surface. The Journal of Physical Chemistry B **2006**, 110, 9188–9194.

- (48) Crespo-Otero, R.; Walsh, A. Variation in Surface Ionization Potentials of Pristine and Hydrated BiVO₄. The Journal of Physical Chemistry Letters **2015**, 6, 2379–2383.
- (49) Ambrosio, F.; Wiktor, J.; Pasquarello, A. pH-Dependent Surface Chemistry from First Principles: Application to the BiVO₄ (010)–Water Interface. ACS Applied Materials & Interfaces **2018**, 10, 10011–10021.
- (50) Hohenberg, P.; Kohn, W. Inhomogeneous Electron Gas. Physical Review **1964**, 136, B864–B871.
- (51) Kohn, W.; Sham, L. J. Self-Consistent Equations Including Exchange and Correlation Effects. Physical Review **1965**, 140, A1133–A1138.
- (52) Schlipf, M.; Gygi, F. Optimization Algorithm for the Generation of ONCV Pseudopotentials. Computer Physics Communications **2015**, 196, 36–44.
- (53) Hamann, D. R. Optimized Norm-Conserving Vanderbilt Pseudopotentials. Physical Review B **2013**, 88, 085117.
- (54) Giannozzi, P. et al. QUANTUM ESPRESSO: A Modular and Open-Source Software Project for Quantum Simulations of Materials. Journal of Physics: Condensed Matter **2009**, 21, 395502.
- (55) Giannozzi, P. et al. Advanced Capabilities for Materials Modelling with Quantum ESPRESSO. Journal of Physics: Condensed Matter **2017**, 29, 465901.
- (56) Dudarev, S. L.; Botton, G. A.; Savrasov, S. Y.; Humphreys, C. J.; Sutton, A. P. Electron-Energy-Loss Spectra and the Structural Stability of Nickel Oxide: An LSDA+U Study. Physical Review B **1998**, 57, 1505–1509.
- (57) Solovyev, I. V.; Dederichs, P. H.; Anisimov, V. I. Corrected Atomic Limit in the Local-Density Approximation and the Electronic Structure of d Impurities in Rb. Physical Review B **1994**, 50, 16861–16871.

- (58) Skone, J. H.; Govoni, M.; Galli, G. Self-Consistent Hybrid Functional for Condensed Systems. Physical Review B **2014**, 89, 195112.
- (59) Sun, W.; Ceder, G. Efficient Creation and Convergence of Surface Slabs. Surface Science **2013**, 617, 53–59.
- (60) Freysoldt, C.; Grabowski, B.; Hickel, T.; Neugebauer, J.; Kresse, G.; Janotti, A.; Van de Walle, C. G. First-Principles Calculations for Point Defects in Solids. Reviews of Modern Physics **2014**, 86, 253–305.
- (61) Freysoldt, C.; Neugebauer, J. First-Principles Calculations for Charged Defects at Surfaces, Interfaces, and Two-Dimensional Materials in the Presence of Electric Fields. Physical Review B **2018**, 97, 205425.
- (62) Cooper, J. K.; Gul, S.; Toma, F. M.; Chen, L.; Liu, Y.-S.; Guo, J.; Ager, J. W.; Yano, J.; Sharp, I. D. Indirect Bandgap and Optical Properties of Monoclinic Bismuth Vanadate. The Journal of Physical Chemistry C **2015**, 119, 2969–2974.
- (63) Kweon, K. E.; Hwang, G. S. Hybrid Density Functional Study of the Structural, Bonding, and Electronic Properties of Bismuth Vanadate. Physical Review B **2012**, 86, 165209.
- (64) Payne, D. J.; Egdell, R. G.; Walsh, A.; Watson, G. W.; Guo, J.; Glans, P.-A.; Learmonth, T.; Smith, K. E. Electronic Origins of Structural Distortions in Post-Transition Metal Oxides: Experimental and Theoretical Evidence for a Revision of the Lone Pair Model. Physical Review Letters **2006**, 96, 157403.
- (65) Zhao, Z.; Li, Z.; Zou, Z. Structure and Energetics of Low-Index Stoichiometric Monoclinic Clinobisvanite BiVO_4 Surfaces. RSC Advances **2011**, 1, 874–883.
- (66) Tachikawa, T.; Ochi, T.; Kobori, Y. Crystal-Face-Dependent Charge Dynamics on

- a BiVO₄ Photocatalyst Revealed by Single-Particle Spectroelectrochemistry. ACS Catalysis **2016**, 6, 2250–2256.
- (67) Li, D.; Liu, Y.; Shi, W.; Shao, C.; Wang, S.; Ding, C.; Liu, T.; Fan, F.; Shi, J.; Li, C. Crystallographic-Orientation-Dependent Charge Separation of BiVO₄ for Solar Water Oxidation. ACS Energy Letters **2019**, 4, 825–831.
- (68) Smondyrev, M. A. Diagrams in the Polaron Model. Theoretical and Mathematical Physics **1986**, 68, 653–664.
- (69) Gerosa, M.; Gygi, F.; Govoni, M.; Galli, G. The Role of Defects and Excess Surface Charges at Finite Temperature for Optimizing Oxide Photoabsorbers. Nature Materials **2018**, 17, 1122–1127.
- (70) Park, H. S.; Kweon, K. E.; Ye, H.; Paek, E.; Hwang, G. S.; Bard, A. J. Factors in the Metal Doping of BiVO₄ for Improved Photoelectrocatalytic Activity as Studied by Scanning Electrochemical Microscopy and First-Principles Density-Functional Calculation. The Journal of Physical Chemistry C **2011**, 115, 17870–17879.
- (71) Hermans, Y.; Murcia-López, S.; Klein, A.; van de Krol, R.; Andreu, T.; Morante, J. R.; Toupance, T.; Jaegermann, W. Analysis of the Interfacial Characteristics of BiVO₄/Metal Oxide Heterostructures and Its Implication on Their Junction Properties. Physical Chemistry Chemical Physics **2019**, 21, 5086–5096.
- (72) Hermans, Y.; Klein, A.; Ellmer, K.; van de Krol, R.; Toupance, T.; Jaegermann, W. Energy-Band Alignment of BiVO₄ from Photoelectron Spectroscopy of Solid-State Interfaces. The Journal of Physical Chemistry C **2018**, 122, 20861–20870.
- (73) Rossell, M. D.; Agrawal, P.; Borgschulte, A.; Hébert, C.; Passerone, D.; Erni, R. Direct Evidence of Surface Reduction in Monoclinic BiVO₄. Chemistry of Materials **2015**, 27, 3593–3600.

- (74) Galembeck, A.; Alves, O. L. BiVO₄ Thin Film Preparation by Metalorganic Decomposition. Thin Solid Films **2000**, 365, 90–93.
- (75) Hamdi, H.; Salje, E. K. H.; Ghosez, P.; Bousquet, E. First-Principles Reinvestigation of Bulk WO₃. Physical Review B **2016**, 94, 245124.
- (76) Seabold, J. A.; Choi, K.-S. Efficient and Stable Photo-Oxidation of Water by a Bismuth Vanadate Photoanode Coupled with an Iron Oxyhydroxide Oxygen Evolution Catalyst. Journal of the American Chemical Society **2012**, 134, 2186–2192.
- (77) Lee, D. K.; Choi, K.-S. Enhancing Long-Term Photostability of BiVO₄ Photoanodes for Solar Water Splitting by Tuning Electrolyte Composition. Nature Energy **2018**, 3, 53–60.

Graphical TOC Entry

